On-Chip Detection of Radiation Power from Flux-Flow Oscillators with Epitaxial and High-J_C NbN/AlN/NbN Junctions

Satoshi KOHJIRO*, Zhen WANG**, Sergey V. SHITOV***, Shigehito MIKI****,
Akira KAWAKAMI**, and Akira SHOJI*
* National Institute of Advanced Industrial Science and Technology,
1-1-4 Umezono, Tsukuba, Ibaraki 305-8568, Japan
** Kansai Advanced Research Center, Communications Research Laboratory,
588-2 Iwaoka, Iwaoka-cho, Nishi-ku, Kobe 651-2492, Japan
*** Institute of Radio Engineering and Electronics,
Mokhovaya 11, 101999 Moscow, Russia
**** Graduate School of Science and Technology, Kobe University,
1-1 Rokkodai-cho, Nada-ku, Kobe 657-8501, Japan

Abstract

To develop an efficient local oscillator (LO) operating above 0.7 THz, the gap frequency of Nb, on a same chip with a SIS mixer, we have investigated the radiation power P of NbN-based flux-flow-type Josephson oscillators (FFOs). The designed and fabricated chip incorporates FFOs, SIS power detectors (DETs), and their coupling circuits. Both FFOs and DETs consist of epitaxial NbN/AlN/NbN junctions with high critical current density J_C ($15 < J_C < 78$ kA/cm^2). The most part of the coupling circuit consists of NbN/SiO_2/Al microstrip lines whose *rf*-loss is approximately 2-3 dB. It has been found P>200 nW, enough for the optimum pumping of a SIS mixer with *rf*-resistance of 50 Ω, is coupled to DETs in the frequency range of 0.5-0.9 THz. The coupling bandwidth is larger than 20% of its central frequency. In the band, the radiation frequency is tuned by the control current through the FFO in the range of 10-100 mA. The peak power >1 μW is detected at 0.76THz. In addition, the dissipated power in a FFO is smaller than 500 μW, which is less than 10^{-4} of that of semiconductor sources. These experimental results indicate that FFOs with high-J_C NbN/AlN/NbN junctions are applicable for an on-chip LO above 0.7 THz.

1. Introduction

For submillimeter-wave astronomy and global monitoring of atmosphere pollution, flux-flow oscillators (FFOs) [1, 2] based on the flux motion in long Josephson junctions

are suitable for a tunable, compact, and low-power consuming local oscillator (LO) on a same chip with a SIS mixer. Recently, Nb-based FFOs were successfully tested as an integrated receiver's LO up to the gap frequency of Nb, say 0.7 THz [3, 4]. To increase the operating frequency of FFOs beyond 0.7 THz, the material of electrodes should be changed. There are two candidates for such electrode material. One is NbTiN grown on several kinds of substrate materials and the other is epitaxial NbN on MgO substrates. Though reported surface resistance of NbTiN film is reasonably low [5] and successfully adopted for the tuning structure in SIS mixers [6, 7], it is difficult to get low dark current when junction electrode is replaced by NbTiN. Epitaxial NbN film [8-10] is suitable not only for the tuning structure [11], but also for NbN/AlN/NbN Josephson junctions with reasonably low dark current in the range of $5<J_C<127$ kA/cm^2 [12], where J_C is the critical current density of Josephson junctions. This feature of epitaxial NbN is an advantage for FFOs and corresponding integrated receivers operating above 0.7 THz. In this paper, we have studied the radiation power P of NbN-based FFOs and demonstrated they are applicable for an on-chip LO above 0.7 THz.

2. Device Design

Fig. 1 shows the top view and cross-section of the device. The designed chip incorporates FFOs, SIS power detectors (DETs), and their coupling circuits. Both FFOs and DETs consist of epitaxial NbN/AlN/NbN junctions with high critical current density J_C ($15<J_C<78$ kA/cm^2).

The FFO's length l_F is 39 or 500 μm, where the former can be used both operational regimes of Fiske resonant and real flux-flow [3, 4], while the resonant mode is completely suppressed above 0.3 THz for l_F=500 μm due to $\alpha l_F>1$, where α is the attenuation constant of electromagnetic wave in a FFO. The FFO's width is W_F=3 μm which does not satisfy the conventional requirement of $W_F<2\lambda_J$ [1] for $J_C>20$ kA/cm^2, where λ_J is its Josephson penetration depth. The reason for adopting W_F=3 μm is that we found in another experiment FFOs with W_F=2 μm become too insensitive to the applied magnetic field to be tuned the oscillation frequency in our interested region. Note that no degradation on characteristics has been experimentally observed for FFOs with $W_F>2\lambda_J$. To obtain steep current steps on its current-voltage characteristics, important both for higher output power and narrower oscillation linewidth, so called projection part with the length of 16 and 100 μm is introduced at the edge of FFOs [2] with l_F=39 and 500 μm, respectively. The bias current of the FFO I_{BF} is fed to the junction due to its overlap geometry, while the control current I_{HF} for applying the

magnetic field flows through the base electrode underneath the FFO.

The length of DETs is 2-3 μm, a half of wavelength in the junction at a certain frequency between 0.55 and 0.82 THz, where the junction capacitance is compensated by the inductance of junction electrodes [13]. The width of DETs is 0.5-2.0 μm to get the variation of their impedance. Both the bias current I_{BD} and the control current I_{HD} for suppression of its Josephson current are supplied to the DET due to its in-line geometry.

The coupling circuit used here is similar to that reported previously [14]. The circuit consists of impedance transformers, a *dc*-break, and *rf*-filters. An impedance transformer with a tapered NbN/SiO_2/Al microstripline matches the output impedance of a FFO (0.5 Ω) to the following circuits of 10-25 Ω. A *dc*-break composed of two microstrip stubs and a pi-slot line in an Al groundplane satisfies both <1 dB coupling loss for *rf*-signal and complete isolation for *dc*-bias between a FFO and a DET. *Rf*-filters are positioned at *dc*-connections for control currents on both DETs and FFOs to prevent the leak of *rf*-signal. The *rf*-loss of the total coupling circuit is estimated as approximately 2-3 dB from our experimental *dc*-properties of epitaxial NbN [10] and Al.

3. Device Fabrication

An epitaxial NbN/AlN/NbN junction sandwich was deposited on a (100) MgO single crystal of 20x20x0.5 mm^3 by an *rf*-magnetron sputtering method without intentional heating of the substrate. The fabrication process of junctions and their characterization were already reported in detail [12]. J_C was varied by the deposition time of the AlN barrier. Thickness of base and counter electrodes was 210-250 and 220-400 nm, respectively. After the sandwich formation, the base electrode was patterned and etched by a reactive ion etching (RIE) technique in CF_4 until the surface of MgO substrate was exposed. Before removing the photoresist, a 250-nm-thick SiO_2 radical absorber was deposited. The role of this radical absorber is explained later. Next, both FFOs and DETs were defined by the patterning and RIE of the counter electrode in CF_4. Since sidewall of base electrodes without the radical absorber was exposed to CF_4 gas plasma, the base electrode was considerably side-etched during the etching of counter electrodes. The above-mentioned SiO_2 radical absorber prevents this side etching, resulting in successful fabrication of 0.5-μm-wide base electrodes. After a 900-nm-thick SiO_2 film was deposited on a whole substrate for an insulation layer, the SiO_2 film was removed with chemical-mechanical polishing technique [15] until the surface of counter electrodes was exposed. This planarization has advantage of both sufficient step coverage over the edge of counter electrodes and ohmic contact between

the wiring and the counter electrode without the formation of small via holes on DETs. The sample was completed by evaporating a 300-nm-thick Al patterned by photoresist stencil lift-off. Typical *dc*-properties of NbN base electrode and Al wiring were as follows. The critical temperature and the normal-state resistivity at 20 K of NbN are 15-16 K and 50-60 μΩcm, respectively. The normal-state resistivity at 20 K and the ratio of resistivities at 300 K and 20 K of Al are 0.2-0.3 μΩcm and 10-20, respectively. These properties are same as those used in a SIS mixer operating above 0.7 THz [11].

4. Results and Discussion

4-1. *Dc*-Characteristics of a FFO and a DET

Current-voltage (I_{BF}-V_F and I_{BD}-V_D) characteristics of fabricated FFOs and DETs were measured at 4.2K with various control currents I_{HF} and I_{HD} for the applied magnetic field, respectively. Fig. 2 shows an example of I_{BF}-V_F characteristic of a FFO with J_C=58 kA/cm^2 and l_F=39 μm. In Fig. 2, current steps are appeared due to the flux-flow in the junction, where each step corresponds to each I_{HF} value. Since the height of current steps I_S is proportional to the generated power in the FFO and step voltage to the oscillation frequency, it is preferable for the higher step to be observed in the wider voltage region. As shown in Fig. 2, I_S >15 mA is clearly observed for 0.6-2.7 mV. It indicates the FFO with epitaxial NbN/AlN/NbN junctions oscillates internally for 0.3-1.3 THz, i.e. close to the gap frequency of the epitaxial NbN. The oscillation frequency is tuned by I_{HF} in the range of 18-86 mA which can be supplied easily from batteries or compact *dc*-power supplies. From I_{BF} and V_F of operating points in Fig. 2, the dissipated *dc*-power in the FFO is estimated <100 μW, since I_{HF} flowing through superconducting base electrode does not consume the power. No FFOs in our experiment consume *dc*-power >500 μW. This value is less than 10^{-4} of that of semiconductor sources such as Gunn diodes used with frequency multipliers.

Fig. 3 shows an example of I_{BD}-V_D characteristic of a DET with J_C=15 kA/cm^2 and the area of 2.9 × 0.5 μm^2. The Josephson current is successfully suppressed by I_{HD}. The solid line denotes the unpumped curve, while the dotted lines pumped ones when the coupled FFO is biased on a current step shown in Fig. 2. As shown, the photon-assisted tunneling (PAT) current is observed for a various bias voltage of coupled FFO V_F. The first PAT step is seen around V_D=1.8 mV. The frequency of the irradiated wave is related to the voltage of the first PAT step V_{PAT1} below V_G as $f_{PAT}=e(V_G-V_{PAT1})/h$, where V_G is the gap voltage of a DET, e the unit charge, and h Planck's constant. From V_G=5.4 mV and V_{PAT1}=1.8 mV, we got f_{PAT}=0.86 THz, which is

consistent with the oscillation frequency of the coupled FFO estimated from V_F as $f_F=2eV_F/h=0.85$ THz.

4-2. *Rf*-Coupling between FFO and DET

Based on the experimental unpumped I_{BD}-V_D curve, theoretical pumped curves are calculated [16] for various *rf*-voltages in the DET V_{rfD}. By fitting the theoretical pumped curve to the experimental one, we get V_{rfD}. From V_{rfD} and the normal resistance of the DET R_{ND}, detected power is calculated as $P=V_{rfD}{}^2/(2R_{ND})$. Fig. 4 shows the detected power as a function of frequency for 5 samples. Each sample has different values of J_C and thickness of SiO_2 insulator t_{SiO2} used in microstrip coupling circuits. For comparison, theoretical power required for the optimum pumping for a SIS mixer with *rf*-resistance of 50 Ω is also plotted as small dots in Fig. 4. As shown, the detected power is larger than the theoretical optimum pumping power between 0.5 and 0.9 THz. The 3dB-bandwidth of each sample is larger than 20% of its central frequency. The peak power of 1.3 μW is detected at 0.76 THz i.e. above the gap frequency of Nb, which indicates the advantage of NbN-based FFOs.

4-3. Optimum J_C

To be clear the preferable J_C values, in Fig. 5, we plot in closed circles the peak value of detected power as a function of J_C. As shown, the peak power increases with J_C and saturates around 70 kA/cm^2. The open squares denote the ratio of junction's subgap resistance at 2mV to its normal resistance R_{ND}, i.e. how small the dark current is. As shown, the normalized dark current is almost independent of J_C below 70 kA/cm^2. From these preliminary results, tentative optimum region of J_C is 50-70 kA/cm^2. This value corresponds to $\omega A_D C_S R_{ND}$ product at 0.7THz of 3-5, which is calculated from J_C-dependent specific capacitance C_S [12] and $J_C A_D R_{ND}=3.75$ mV which is experimentally obtained, where ω is the angular frequency and A_D the area of DETs. This $\omega A_D C_S R_{ND}$ value is also suitable for the design of SIS mixers on a same chip with FFOs. For practical application, further discussion on optimum J_C will be necessary from the view point of J_C-dependent oscillation linewidth of FFOs [17].

4-4. Upper Frequency Limitation

Fig. 6 shows the relation between the maximum coupling frequency f_{MC} and t_{SiO2} used in microstrip coupling circuits, where the inset shows the definition of f_{MC}. The

solid line denotes the designed value and triangles the experimental ones. As shown, the experimental f_{MC} is 10-20% smaller than the designed value. To study the reason of this discrepancy, in Fig. 7, we compare the experimental (triangles with line) and theoretical (solid curve) frequency-dependent power transmissions from a FFO to a DET, where two types of microstrip coupling circuits are adopted. The insets show the configuration of microstrip lines.

Fig 7 (a) shows the case of normal microstrip line used for our present design. The electric field in the line concentrates under the stripline. The contribution to the line capacitance of the free space behind the stripline is negligibly small because of its low dielectric constant (ε_r=1) though weak electric field exists in the free space. Note that a substrate behind the groundplane never contributes since the electric field does not exist in a substrate. Using this model for the calculation, we find the discrepancy between theoretical and experimental frequency responses.

Fig. 7 (b) shows the case of embedded microstrip line closer to our device configuration shown in Fig. 1 (b). A MgO substrate with ε_r=9.6 is attached not behind the groundplane but behind the stripline. Because of the electric field in the substrate, the substrate increases the line capacitance, i.e. decreases f_{MC} from the initial value of the normal type. As a result, theoretical value fits reasonably experimental one.

In Fig. 6, the designed f_{MC} based on embedded microstrip circuits is also plotted in open squares, which agree quantitatively with experimental value. These results indicate f_{MC} of the present experiment is determined not by FFOs but by microstrip parameters far from the optimum value. It suggests the future possibility of detection of required power for 0.9-1.3 THz after redesigning the coupling circuit based on the embedded microstrip model.

5. Conclusion

We have demonstrated the radiation power P>200 nW from NbN-based FFOs is detected by on-chip SIS detectors for 0.5-0.9 THz. The peak power >1 μW is detected above the gap frequency of Nb. The coupling bandwidth is larger than 20% of its central frequency. In the band, the radiation frequency is tuned by the control current through the FFO in the range of 10-100 mA. The dissipated power in a FFO is less than 500 μW. Higher J_C is preferable for larger P. The maximum detectable frequency is determined by parameters of microstrip coupling circuits. These experimental results indicate that FFOs with high-J_C NbN/AlN/NbN junctions are applicable for an on-chip local oscillator above 0.7 THz.

Acknowledgements

The authors would like to acknowledge M. Takeda in Communications Research Laboratory and T. Noguchi in Nobeyama Radio Observatory, Japan, for the guidance of the calculation of pumped *I-V* curves of DETs. They thank the members of Superconducting Devices Group and Microsystems Group in AIST for the management of facilities required for this work. J. Itoh is appreciated for continuous support and encouragement. This work is supported in part by the Ministry of Education, Culture, Sports, Science and Technology, Japan and a fellowship program by Japan Society for the Promotion of Science, as well as RFBR (Russian Foundation for Basic Research) projects 00-02-16270 and INTAS (INTernational ASsociation for Promotion of the Scientific Research in Russia funded by NATO countries) project 01-0367.

References

[1] T. Nagatsuma, K. Enpuku, K. Yoshida, and F. Irie "Flux-flow-type Josephson oscillator for millimeter and submillimeter wave region. II. Modeling", *J. Appl. Phys.* **56**, 3284-3293 (1984).

[2] T. Nagatsuma, K. Enpuku, K. Sueoka, K. Yoshida, and F. Irie "Flux-flow-type Josephson oscillator for millimeter and submillimeter wave region. III. Oscillation stability", *J. Appl. Phys.* **58**, 441-449 (1985).

[3] V. P. Koshelets and S. V. Shitov, "Integrated superconducting receivers", *Supercond. Sci. Technol.* **13**, R53-R69 (2000).

[4] V.P. Koshelets and J. Mygind, "Flux flow oscillators for superconducting integrated submm wave receivers", *Studies of High Temperature Superconductors*, edited by A.V. Narlikar, NOVA Science Publishers, New York, **39,** 213-244 (2001).

[5] J. W. Kooi, J. A. Stern, G. Chattopadhyay, H. G. LeDuc, B. Bumble, and J. Zmuidzinas, "Low-loss NbTiN films for THz SIS mixer tuning circuits", *Int. J. Infrared Millim. Waves* **19**, 373 (1998).

[6] J. Kawamura, J. Chen, D. Miller, J. Kooi, J. Zmuidzinas, B. Bumble, H. G. LeDuc, and J. A. Stern, "Low-noise submillimeter-wave NbTiN superconducting tunnel junction mixers", *Appl. Phys. Lett.* **75**, 4013-4015 (1999).

[7] B. D. Jackson, A. M. Baryshev, G. de Lange, J. R. Gao, S. V. Shitov, N. N. Iosad, and T. M. Klapwijk, "Low-noise 1THz superconductor-insulator-superconductor mixer incorporating a NbTiN/SiO_2/Al tuning circuit", *Appl. Phys. Lett.* **79**, 436-438 (2001).

[8] A. Shoji, S. Kiryu, and S. Kohjiro, "Superconducting properties and normal-state

resistivity of single-crystal NbN films prepared by a reactive rf-magnetron sputtering method", *Appl. Phys. Lett.* **60**, 1642-1626 (1992).

[9] Z. Wang, A. Kawakami, Y. Uzawa, and B. Komiyama, "Superconducting properties and crystal structures of single-crystal niobium nitride thin films deposited at ambient substrate temperature", *J. Appl Phys.* **79**, 7837-7842 (1996).

[10] S. Kohjiro and A. Shoji, "Surface resistance of NbN and NbC_xN_{1-x} films in the frequency range of 0.5-1.5THz", *Inst. Phys. Conf. Ser.* No **167**, IOP Publishing Ltd., 655-658 (2000). S. Kohjiro, S, Kiryu, and A. Shoji, "Surface resistance of epitaxial and polycrystalline NbCN films in submillimeter wave region", *IEEE Trans. Appl. Supercond.* **3**, 1765-1767 (1993).

[11] Y. Uzawa, Z. Wang, and A. Kawakami, "Terahertz NbN/AlN/NbN mixers with Al/SiO/NbN microstrip tuning circuits", *Appl. Phys. Lett.* **73**, 680-682 (1998).

[12] Z. Wang, H. Terai, A. Kawakami, Y. Uzawa, "Characterization of NbN/AlN/NbN Tunnel Junctions", *IEEE Trans. Appl. Supercond.* **9**, 3259-3262 (1999).

[13] V. Yu Belitsky, E. L. Kollberg, "Superconductor-insulator-superconductor tunnel strip line: Features and applications", *J. Appl. Phys.* **80**, 4741-4748 (1996).

[14] S. V. Shitov, V. P. Koshelets, L. V. Filippenko, P. N. Dmitriev, V. L. Vaks, A. M. Baryshev, W. Luinge, N. D. Whyborn, and J. R. Gao, "A superconducting integrated receiver with phase-lock loop", *Inst. Phys. Conf. Ser.* No **167**, IOP Publishing Ltd., 647-650 (2000).

[15] S. Kohjiro, H. Yamamori, and A. Shoji, "Fabrication of niobium-carbonaitride Josephson junctions on magnesium-oxide substrates using chemical-mechanical polishing", *IEEE Trans. Appl. Supercond.* **9**, 4464-4466 (1999).

[16] C. A. Hamilton and S. Shapiro, "Rf-induced effects in superconducting tunnel junctions", *Phys. Rev. B* **2**, 4494-4503 (1970).

[17] V. P. Koshelets, private communication.

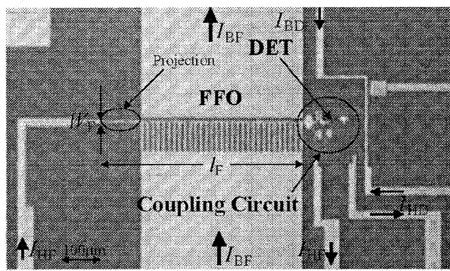

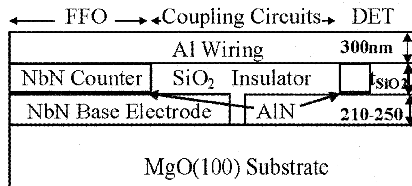

Fig. 1. Top view (a) and cross-section (b) of a FFO and a coupled DET. Al wiring is not shown in (a).

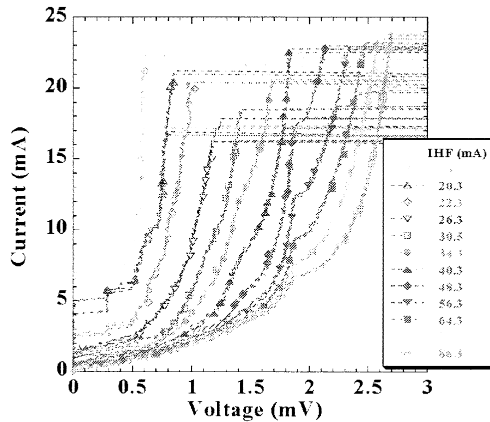

Fig. 2. I_{BF}-V_F characteristics of a FFO with J_C=58kA/cm^2, l_F=39 μm, and W_F=3 μm under various control currents I_{HF}.

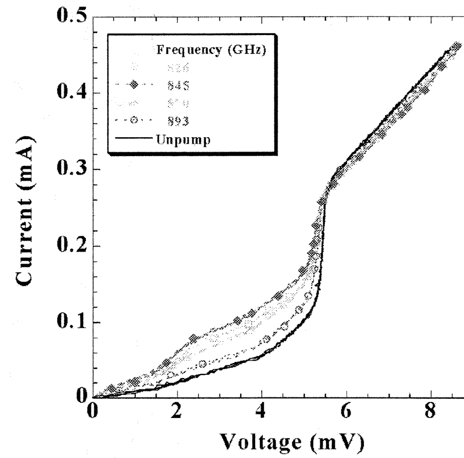

Fig. 3. I_{BD}-V_D curves of a DET with J_C=15kA/cm^2 and area of 2.9 x 0.5 μm^2 under various oscillation frequency of the coupled FFO.

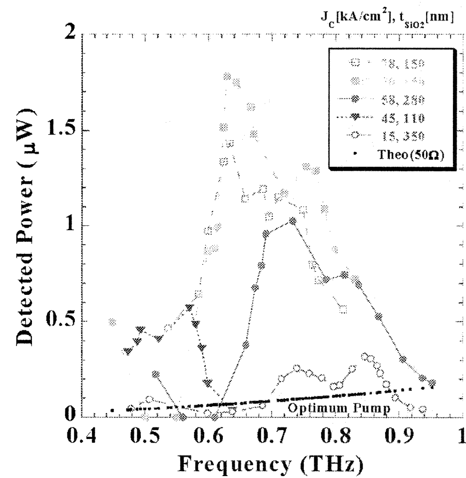

Fig. 4. Detected power P vs. oscillation frequency of FFOs. Experimental results on 5 samples with various J_C and t_{SiO2} are shown. Theoretical optimum pumping power for a SIS mixer with *rf*-resistance of 50 Ω is plotted in small dots.

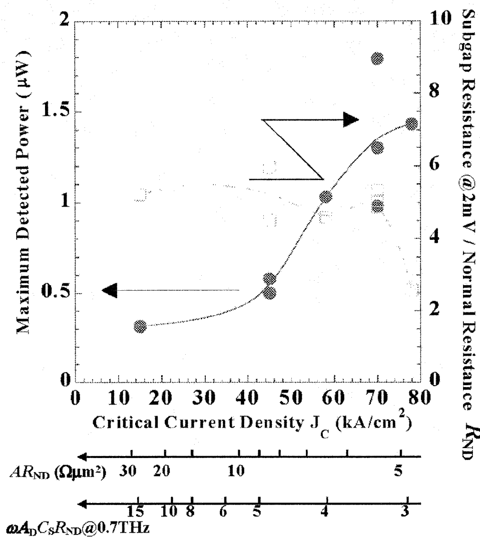

Fig. 5. Peak power (closed circles) and ratio of subgap resistance at 2mV to normal resistance (open squares) vs. J_C. The horizontal axis is also on scales of $A_D R_{ND}$ and $\omega A_D C_S R_{ND}$ products at 0.7THz.

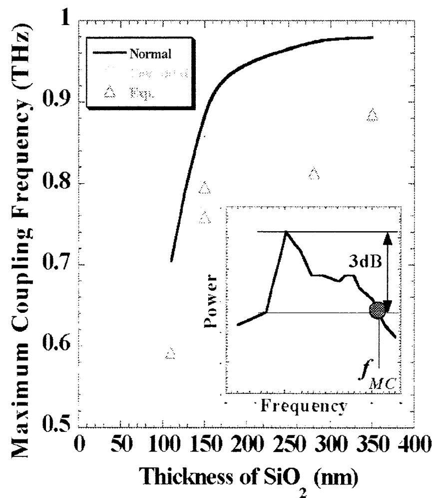

Fig. 6. Maximum coupling frequency f_{MC} vs. t_{SiO2} for designed and experimental (triangles) values. Designed f_{MC} is calculated both for normal (solid line) and embedded (squares) microstrip coupling circuits shown in Fig. 7. The inset shows the definition of f_{MC}.

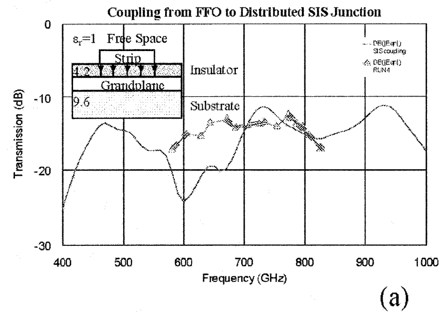

(a)

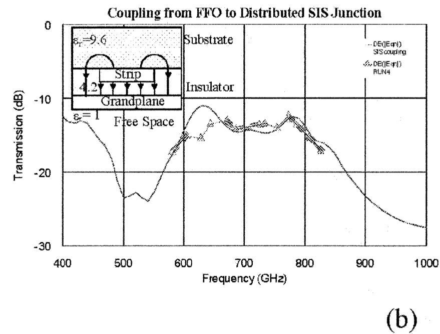

(b)

Fig. 7. Frequency dependence of power transmission from a FFO to a DET for designed (solid line) and experimental (triangles with line) values. Designed value is based on (a) normal and (b) embedded microstrip coupling circuits. Inset shows the configuration of microstrip lines.